

# Novel circularly polarized slot array antennas with a wide 3-dB axial ratio bandwidth based on a spindle-shaped radiating cavity

Hai Wang<sup>1</sup> , Xue Lei<sup>1,2</sup>, Tiandong Duan<sup>1</sup>, Tianpeng Li<sup>1,2</sup>, Jun Gao<sup>1,2</sup>  
and Mingyang Zhao<sup>1,3</sup>

## Research Paper

**Cite this article:** Wang H, Lei X, Duan T, Li T, Gao J, Zhao M (2023). Novel circularly polarized slot array antennas with a wide 3-dB axial ratio bandwidth based on a spindle-shaped radiating cavity. *International Journal of Microwave and Wireless Technologies* **15**, 486–492. <https://doi.org/10.1017/S1759078722000320>

Received: 6 October 2021  
Revised: 14 February 2022  
Accepted: 19 February 2022  
First published online: 28 March 2022

### Key words:

Array antenna; axial ratio bandwidth; circularly polarized; spindle-shaped coupling cavity

### Author for correspondence:

Hai Wang,  
E-mail: [wh839459262@foxmail.com](mailto:wh839459262@foxmail.com)

<sup>1</sup>Information Engineering University, Zhengzhou, China; <sup>2</sup>National Digital Switching System Engineering and Technological R&D Center, Zhengzhou, China and <sup>3</sup>State Key Laboratory of Complex Electromagnetic Environment Effects on Electronics and Information System, Luoyang, China

### Abstract

A novel wide 3-dB axial ratio (AR) circularly polarized  $2 \times 2$  array antenna is proposed in this paper. The spindle-shaped coupling cavity with tilted waveguide is capable of generating circular polarization waves from incident linear waves, which improves the AR bandwidth (ARBW) of the antenna. With this structure, a similar amplitude of the two orthogonal transmitted wave components and a stable phase difference of nearly  $90^\circ$  can be generated. The circularly polarized antenna proposed herein has been fabricated. According to the measurement results, the operating bandwidth from 5.32 to 6.13 GHz is  $< -10$  dB. In addition, the measured ARBW, which is below 3 dB, can cover the range of 5.41–6.02 GHz. The maximum gain of the antenna can attain 15.65 dBi, and the efficiency is better than 80%.

## Introduction

Circularly polarized antennas are critical for high-performance and low-loss antenna applications, such as uncompressed high-definition media transfers, sensing systems, and long-range high-resolution radar systems [1]. Circularly polarized antennas, offering desirable advantages such as flexibility, mobility, weather penetration, and reduction in multipath reflections in transmission and reception, will be employed more widely in these systems [2]. A waveguide slot antenna demonstrates the merits of high efficiency, low cost, and flexible mechanical assembly. To improve the operating bandwidth and radiation efficiency, the patch is covered on the waveguide slot antenna in [3], but the axial ratio bandwidth (ARBW)  $< 3$  dB is only 3%. In [4, 5], parasitic dipoles are placed above the gap to achieve circular polarization (CP). A major difference between [4] and [5] is that in [5] three parasitic patches are placed on the substrate waveguide. The antenna in [6] consists of a pair of loops fed by a slot and two square patches are added on the opposite corners of both loops to implement CP. In [7, 8], an antenna is filled with a dielectric material in the waveguide. The impedance bandwidth (IBW) and ARBW performance of the antenna can be effectively improved. However, the substrate loss will become worse with the increase in frequency and expansion of the array. The authors in [9] used a combination of slots with different lengths to expand the IBW and ARBW of the antenna, achieving a 21% wider ARBW, and a lower gain with seven elements. In [10], a circular polarizer is added to each slot of a waveguide slot antenna with a CP bandwidth of 2%. In [11], CP is realized by combining two orthogonal linear polarizations, which are generated by two pairs of radiation slots on a cavity surface. However, the ARBW of the antenna is only 1.2%. The circular polarizer is fed by a slot, but the ARBW is narrow in [12–14].

In this paper, we designed a wide-axis ratio antenna that can achieve CP. The antenna is an all-metal structure, which is relatively simple to process and of low cost. The adopted coupling cavity with a twisted waveguide effectively improves the CP axis ratio performance of the antenna. The three-dimensional model of the antenna is shown in Fig. 1.

## CP unit cell design

In [15], a microstrip circularly polarized antenna is designed. The rectangular strips form an orthogonal current with a  $90^\circ$  time shift on the surface of the antenna. The structure composed of two symmetrical square-coupling cavities is designed in this paper, which can form an electric field with a  $90^\circ$  time shifted. The unit is shown in Fig. 2. A symmetric square-coupling cavity is placed on a waveguide ( $F_1 \times F_2$ ) and excited. The operating principle of the CP antenna is that two orthogonal electric field modes with equal amplitude but a phase shift of  $90^\circ$  can be obtained [16]. The symmetric square-coupling cavity is connected by two square-coupling

© The Author(s), 2022. Published by Cambridge University Press in association with the European Microwave Association. This is an Open Access article, distributed under the terms of the Creative Commons Attribution licence (<https://creativecommons.org/licenses/by/4.0/>), which permits unrestricted re-use, distribution, and reproduction in any medium, provided the original work is properly cited.

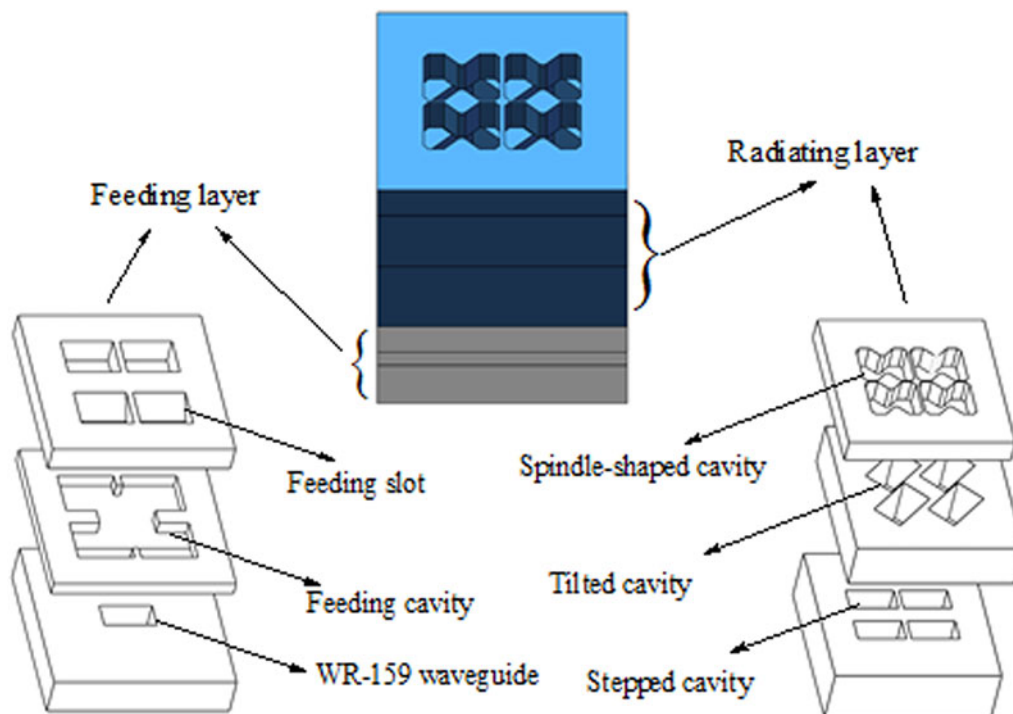


Fig. 1. Configuration of the proposed coupling cavity 2 × 2 CP array antenna.

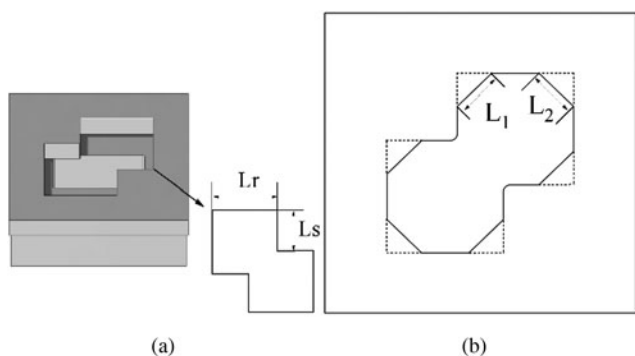


Fig. 2. Views of the proposed unit cell: (a) symmetric square-coupling cavity and (b) spindle-shaped cavity ( $L_1 = 9.16$  mm,  $L_2 = 20$  mm).

cavities, as shown in Fig. 2(a). However, the size of the configuration will not make the distance between the array elements less than one wavelength. The corners of the symmetrical square-coupling cavity are cut to improve the compactness of the antenna. Figure 2(b) shows a spindle-shaped coupling cavity. The comparison simulated results of  $S_{11}$  and AR of the two structures are shown in Fig. 6.

The electric field of the waveguide is coupled to the symmetric square-coupling cavity, where it is decomposed into orthogonal electric fields with the same amplitude and  $90^\circ$  phase shift. Figure 3 shows the electric field of the unit cell operating at 5.8 GHz. The electric field density on the surface of the antenna for different phases of excitation field is simulated. When the phase of the excitation vector is  $0^\circ$  or  $180^\circ$  and  $90^\circ$  or  $270^\circ$ , which gives rise to radiation of waves polarized along the  $x$ -axis and  $y$ -axis and obtain the right-handed circularly polarized (RHCP) electric field.

To demonstrate the effects of these parameters, we analyzed the axial ratio (AR) of the antenna with different values of  $L_r$  and  $L_s$ . The dependences of the AR on the different values at the lower frequency band and the higher frequency band are presented in Figs 4(a) and 4(b), respectively. If the value of  $L_r$  is  $< 0.6\lambda_0$  (where  $\lambda_0$  is the free-space wavelength at 5.8 GHz), the AR curve will be shifted. The AR performance will become worse when the value of  $L_r$  is more than  $0.6\lambda_0$ . The best value for the CP axis ratio performance is  $L_s = 0.4\lambda_0$ . When the sum of  $L_r$  and  $L_s$  is  $\lambda_0$ , the best CP axis ratio performance can be obtained. The ARBW of 14.6% can be achieved by the unit. Figure 6 shows the  $S_{11}$  and AR curves of two coupling cavities. It is found by comparison that the performance of the spindle-shaped coupling cavity is preferable.

### 2 × 2 Array antenna design

#### Feeding and coupling layer design

The feeding design of the antenna adopts the same method as [17], and the structural parameters are shown in Table 1. If the distance between the antenna elements is less than one wavelength, the antenna sidelobe level will decrease [18]. Note that the distance between the feeding slots should accommodate four subarrays next to each other, while being compact enough to ensure proper spacing for the radiating slots to avoid a high grating lobes' effect. The distance between the array elements is more than  $\lambda_0$  if the spindle-shaped coupling cavity is directly excited by the feeding port.

The antenna adopts a combined structure of stepped design and tilted design as shown in Fig. 5. The size of the tilted waveguide is  $T_1 \times T_w$  twisted by  $45^\circ$ , which decomposes the electric field into horizontal and vertical components. The electric field is further decomposed to obtain an orthogonal electric field

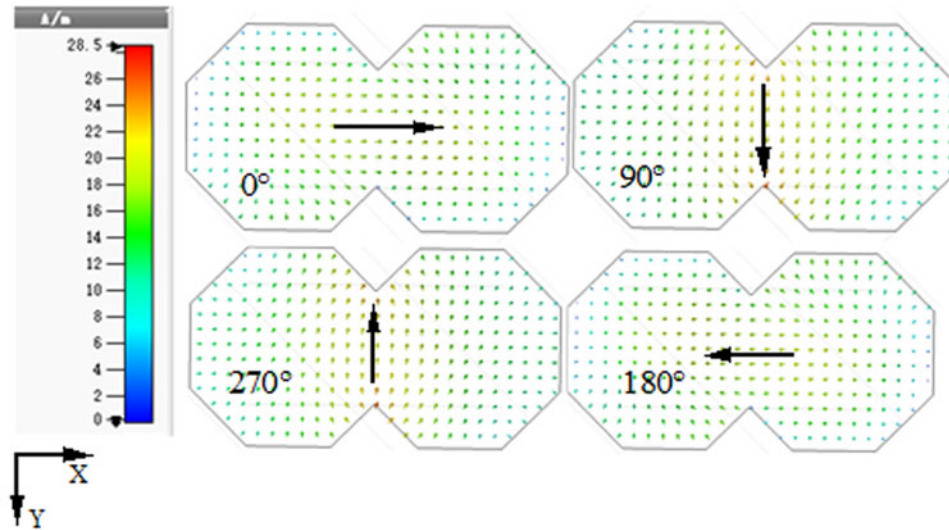
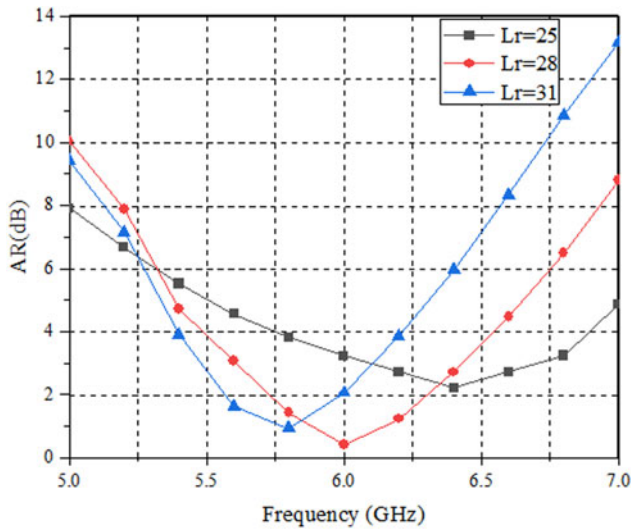
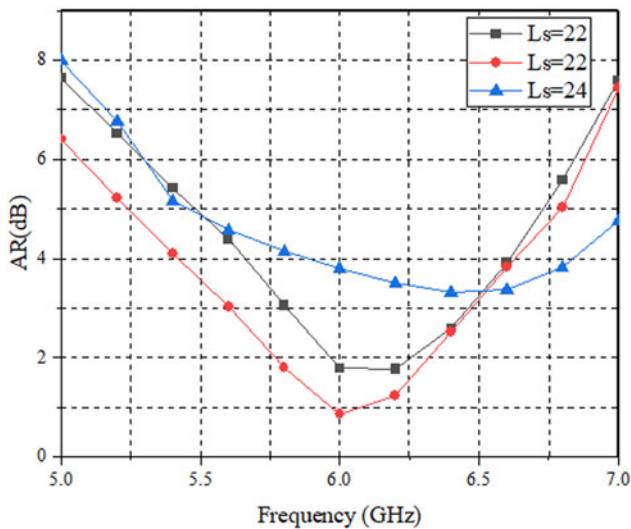


Fig. 3. Electric field distributions of the coupling slots at 5.8 GHz.



(a)



(b)

Fig. 4. Simulation of the  $L_r$  and  $L_s$ : (a) AR for different values of  $L_r$  and (b) AR for different values of  $L_s$ .

Table 1. Optimized parameters of the array antenna

Parameters	$W_1$	$W_2$	$W_{p1}$	$W_{p2}$	$S_1$	$S_2$
Values (mm)	85	90	5	13	15	7
Parameters	$F_l$	$F_w$	$F_s$	$R_l$	$R_w$	$T_l$
Values (mm)	38	17	5	40	17	45
Parameters	$T_w$	$C_l$	$C_w$	$h_1$	$h_2$	$h_3$
Values (mm)	21	42	32	20	30	25

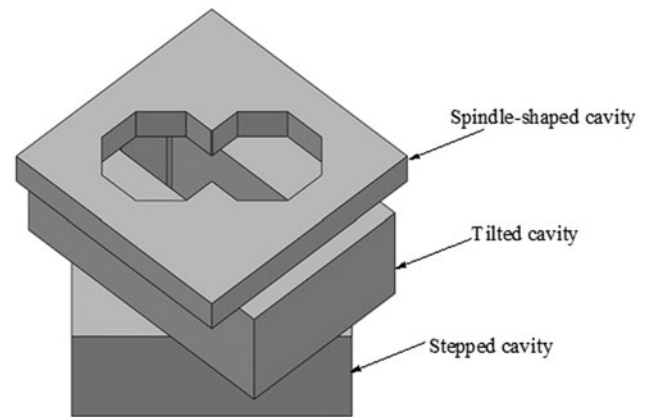


Fig. 5. Spindle-shaped cavity with tilted waveguide.

with equal amplitude and  $90^\circ$  phase shift in the spindle-shaped cavity. A comparison with the former result is shown in Fig. 6. The AR is expanded to 17%.

### Array antenna design

Two parts constitute the antenna, including the feeding layer and the coupling layer. As shown in Fig. 1, four radiating elements in free space are positioned symmetrically in free space in the  $x$ - and  $y$ -directions. The distances between the coupling cavities are  $F_s$

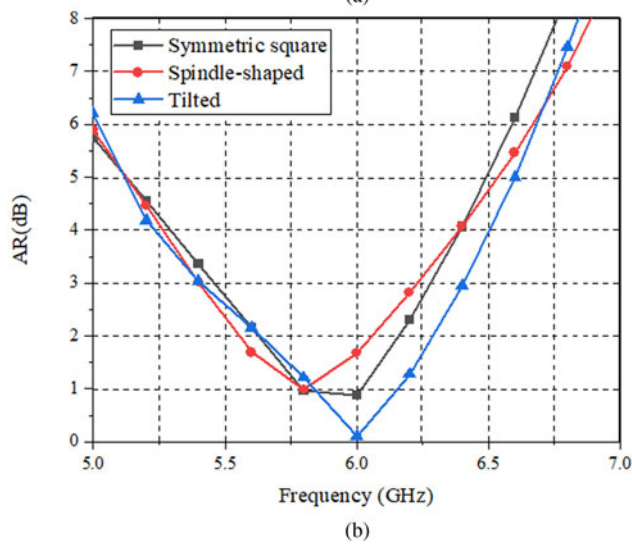
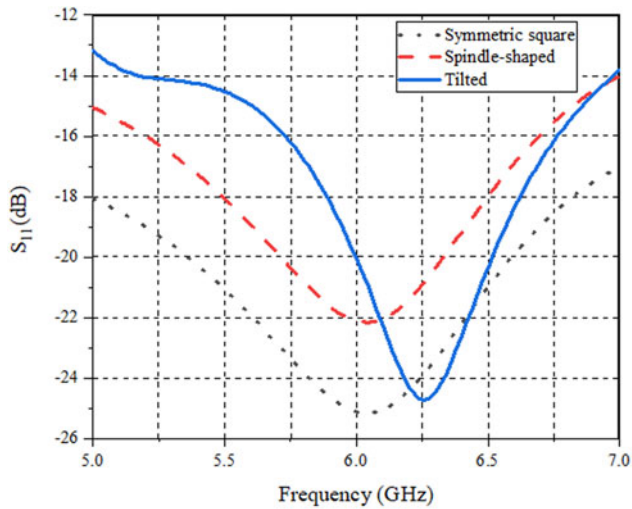


Fig. 6. Simulated with different cavities: (a)  $S_{11}$  and (b) AR.

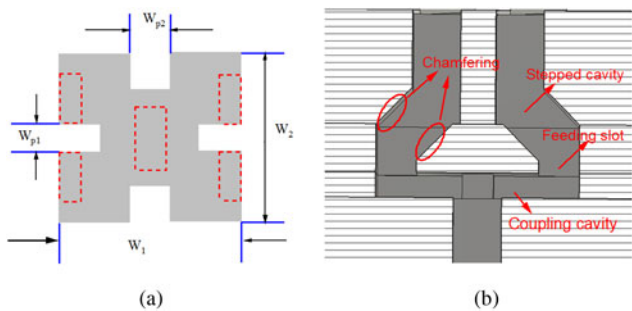


Fig. 7. (a) Views of the feeding layer. (b) Views of the chamfering.

and  $S_1$ . Figures 7 and 8 show the whole configuration of the multistep profile. The red dotted lines at the corners of the four cavities show the exact position of each radiating element relative to the groove in the center of the cavity. The overall structure is shown in Fig. 7. The stepped design and tilted design make the antenna more compact on the  $y$ -axis. The offset of the stepped layer is  $S_2$ . The feeding port and the stepped layer are connected

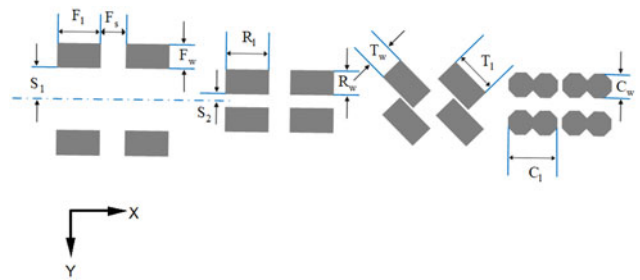


Fig. 8. Multi-stepped configuration of the antenna.

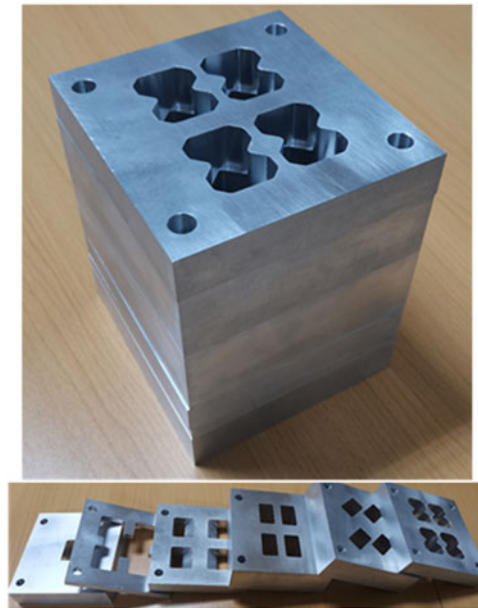
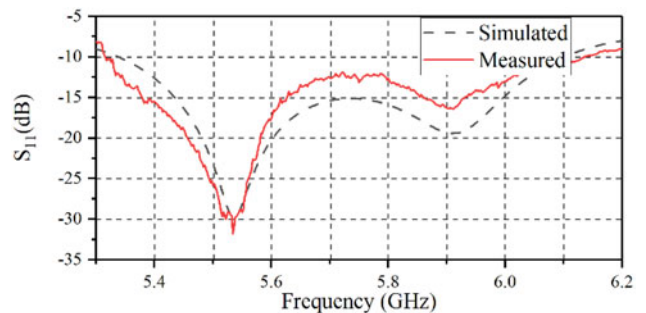
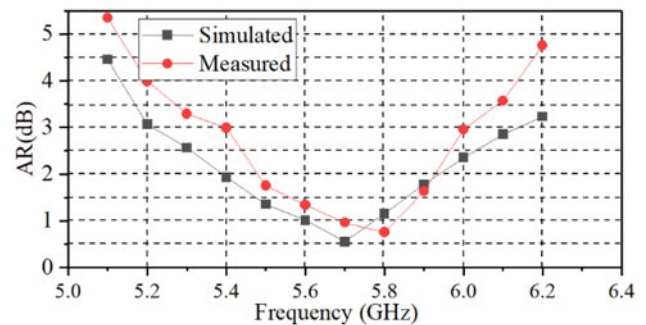


Fig. 9. Fabrication of the antenna.



(a)



(b)

Fig. 10. Simulated and measured results: (a)  $S_{11}$  and (b) AR.

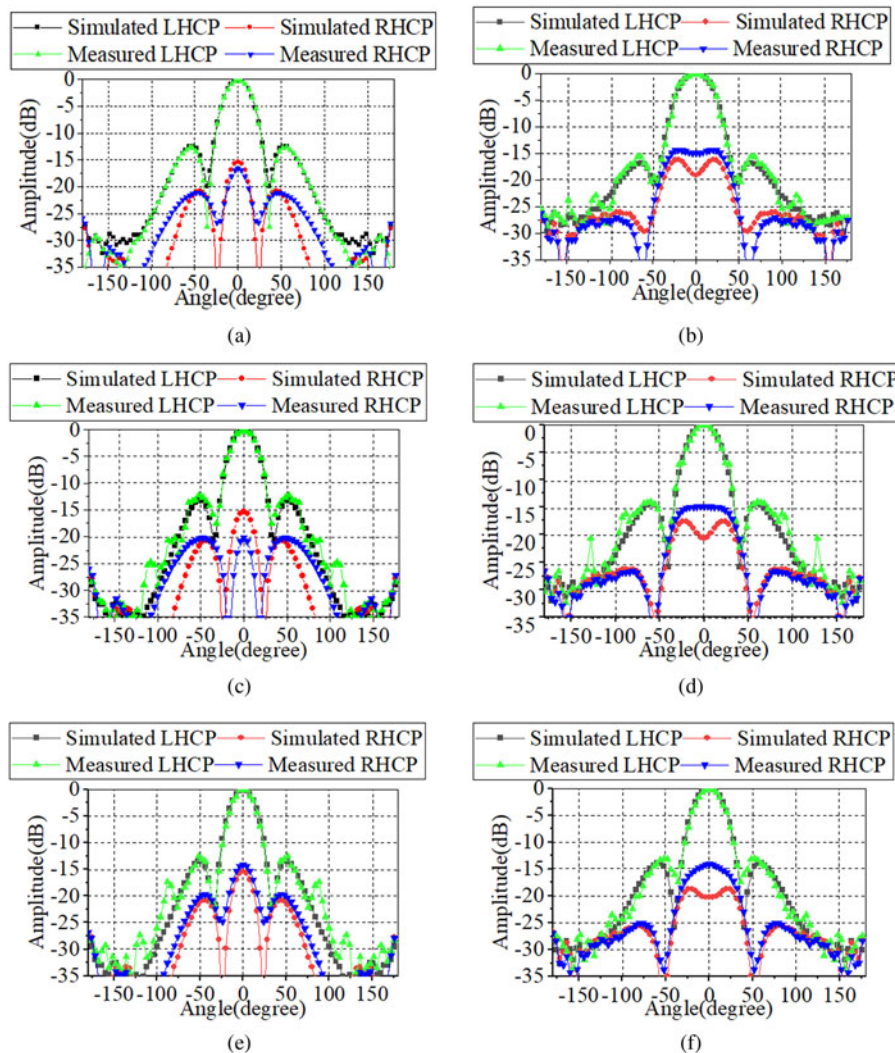


**Fig. 11.** Simulated and measured radiation patterns in the *E*- and *H*-planes: (a) *E*-plane at 5.5 GHz, (b) *H*-plane at 5.5 GHz, (c) *E*-plane at 5.7 GHz, (d) *H*-plane at 5.7 GHz, (e) *E*-plane at 5.9 GHz, and (f) *H*-plane at 5.9 GHz.

by chamfering to improve impedance matching, as shown in Fig. 7(b). The sidelobe level of the *E* side is below  $-12.65$  dB, and the minimum sidelobe level of the *H* side can attain  $-15.54$  dB.

**Simulated and measured results**

To verify the design, the  $2 \times 2$  element antenna array was fabricated as shown in Fig. 9. The curve in Fig. 10 shows the measured and simulated  $S_{11}$  and AR curves: the CP AR is below 3 dB at 5.41–6.02 GHz. Due to the mutual interference between the array elements, the ARBW of the CP array antenna is only 10.6%. As shown, the measurement and simulation results agree quite well with only a slight shift due to the fabrication tolerances.

Each element of the antenna radiates evenly. Compared with a traditional waveguide slot array antenna, the beam of the antenna is always in the normal phase [19]. The simulated RHCP and left-hand circularly polarization patterns of 5.5, 5.7, and 5.9 GHz in the *E*- and *H*-planes are shown in Fig. 12. The radiation patterns of 5.5, 5.7, and 5.9 GHz in the *E*- and *H*-planes are shown in Fig. 11. The sidelobe levels of the antenna measured on the *E*-plane are  $-12.7$ ,  $-12.65$ , and  $-13.05$  dB; on the *H*-plane, the sidelobe levels are  $-15.54$ ,  $14.05$ , and  $-13$  dB due to the large distance between the array elements. It can be seen from Fig. 12 that

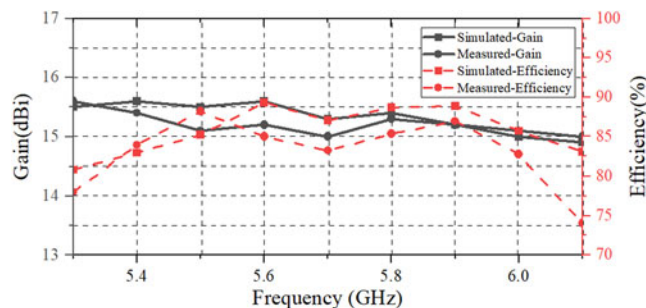


**Fig. 12.** Efficiency and gain of the array antenna.

**Table 2.** Comparison with some previous works

Ref.	Number of the elements	ARBW (%)	IBM (%)	Gain (dBi)
[1]	$1 \times 10$	3.2	4	15.94
[4]	$1 \times 10$	1.4	1.76	15.4
[9]	$1 \times 7$	21	27	12.5
[10]	$1 \times 1$	1.2	6.6	9.8
Our work	$2 \times 2$	10.6	14.7	15.65

the measured antenna-radiating efficiency is above 80% in the working bandwidth. The maximum antenna gain can attain 15.65 dBi.

The asymmetric structure would increase the loss of the antenna, the insertion loss of each port is 6.08 dB at 5.8 GHz. Compared with the traditional waveguide slot antenna, the antenna has a wider ARBW. This antenna has lower loss compared to the substrate waveguide slot antenna. In [20], the length of the circular polarizer is  $\lambda_0$ , while the length of the cavity proposed in this paper is only  $0.36\lambda_0$ . Table 2 shows a comparison with the performances of the antennas in several literature studies.

## Conclusion

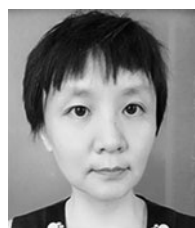
In this paper, a circularly polarized  $2 \times 2$  array antenna based on a spindle-shaped radiation cavity is proposed. The antenna has the advantages of high efficiency, wide ARBW, and low cost. The comparison of the three design methods demonstrates that adding the tilted waveguide can effectively improve the ARBW of the antenna to enhance the CP characteristics. Finally, the new CP antenna adopts the stepped design and the tilted design, which have wide IBW and ARBW as well as a good gain.

## References

1. Cheng YJ, Guo YX and Liu ZG (2014) W-band large-scale high-gain planar integrated antenna array. *IEEE Transactions on Antennas and Propagation* **62**, 3370–3373.
2. Bai X, Qu S, Yang S, Hu J and Nie Z (2016) Millimeter-wave circularly polarized tapered-elliptical cavity antenna with wide axial-ratio beamwidth. *IEEE Transactions on Antennas and Propagation* **64**, 811–814.
3. Xu J, Wang M, Huang H and Wu W (2015) Circularly polarized patch array fed by slotted waveguide. *IEEE Antennas and Wireless Propagation Letters* **14**, 8–11.
4. Keivaan A, Oraizi H and Amini A (2018) Design of circularly-polarized cavity-backed slot array antenna using higher-order mode excitation based on gap waveguide technology. *9th International Symposium on Telecommunications (IST)*, pp. 535–537.
5. Ferrando-Rocher M, Herranz-Herruzo JJ, Valero-Nogueira A and Rodrigo VM (2016) Circularly polarized slotted waveguide array with improved axial ratio performance. *IEEE Transactions on Antennas and Propagation* **64**, 4144–4148.
6. Lu L, Jiao Y, Weng Z, Zhang H and Cui C (2017) Design of low-sidelobe circularly polarized loop linear array fed by the slotted SIW. *IEEE Antennas and Wireless Propagation Letters* **16**, 537–540.
7. Bai X, Qu S and Chan C (2016) Circularly polarized series-fed patch array for THz applications. *IEEE International Symposium on Antennas and Propagation (APSURSI)*, pp. 595–596.
8. Zhao Y and Luk K (2018) Dual circular-polarized SIW-fed high-gain scalable antenna array for 60 GHz applications. *IEEE Transactions on Antennas and Propagation* **66**, 1288–1298.
9. Al Sharkawy M and Kishk AA (2014) Wideband beam-scanning circularly polarized inclined slots using ridge gap waveguide. *IEEE Antennas and Wireless Propagation Letters* **13**, 1187–1190.
10. Chen Q, Wu T, Wan Y, Li L and Jin M (2019) A circularly polarized waveguide slot antenna for random array application. *International Conference on Microwave and Millimeter Wave Technology (ICMMT)*, pp. 1–3.
11. Wu X, Yang F, Xu F and Zhou J (2017) Circularly polarized waveguide antenna with dual pairs of radiation slots at Ka-band. *IEEE Antennas and Wireless Propagation Letters* **16**, 2947–2950.
12. Wang Y, Zhu F and Gao S (2020) Design of a simple circularly polarized antenna for millimeter-wave applications. *13th UK-Europe-China Workshop on Millimetre-Waves and Terahertz Technologies (UCMMT)*, pp. 1–3.
13. Al-Saedi H, Abdel-Wahab W, Raeis-Zadeh SM, Gigoyan S and Safavi-Naeini S (2017) A wide axial ratio beamwidth circularly polarized antenna for Ka-band satellite on the move (SOTM) phased array applications. *IEEE International Symposium on Antennas and Propagation and UNSC/URSI National Radio Science Meeting*, pp. 2557–2558.
14. Gharibi H and Hodjatkashani F (2015) Design of a compact high-efficiency circularly polarized monopulse cavity-backed substrate integrated waveguide antenna. *IEEE Transactions on Antennas and Propagation* **63**, 4250–4256.
15. Xu R, Li J, Qi Y, Guangwei Y and Yang J (2017) A design of triple-wideband triple-sense circularly polarized square slot antenna. *IEEE Antennas and Wireless Propagation Letters* **16**, 1763–1766.
16. Hesari SS and Bornemann J (2017) Wideband circularly polarized substrate integrated waveguide endfire antenna system with high gain. *IEEE Antennas and Wireless Propagation Letters* **16**, 2262–2265.
17. Shad S and Mehrpouyan H (2020) 60 GHz waveguide-fed cavity array antenna by multisteped slot aperture. *IEEE Antennas and Wireless Propagation Letters* **19**, 438–442.
18. Chu H, Li P and Guo Y (2019) A beam-shaping feeding network in series configuration for antenna array with cosecant-square pattern and low sidelobe. *IEEE Antennas and Wireless Propagation Letters* **18**, 742–746.
19. Wang E, Zhang T, He D, Chen L and Yang J (2019) Wideband high-gain circularly polarized antenna array on gap waveguide for 5G applications. *International Symposium on Antennas and Propagation (ISAP)*, pp. 1–3.
20. Lu X, Gu S, Wang X, Liu H and Lu W (2017) Beam-scanning continuous transverse stub antenna fed by a ridged waveguide slot array. *IEEE Antennas and Wireless Propagation Letters* **16**, 1675–1678.



**Hai Wang** received his BS degree from Logistical Engineering University, Chongqing, China, in 2015. He is currently working at PLA Strategic Support Information Engineering University pursuing his MS degree. His main research interests include aperture antennas, wideband antennas, and wide axial ratio antennas.



**Xue Lei** received her BS and MS degrees from PLA Strategic Support Information Engineering University, Zhengzhou, China, in 1989 and 2000, respectively. She is currently working at PLA Strategic Support Information Engineering University. Her main research interests include antennas and propagation.



**Tiandong Duan** received his BS and MS degrees from the Army Engineering University of PLA, Nanjing, China, in 1989 and 2000, respectively. He is currently working at PLA Strategic Support Information Engineering University. His main research interests include signal processing.



**Tianpeng Li** received his BS and MS degrees from Air Force Engineering University, Xi'an, China, in 2012 and 2016, respectively. He is currently working at PLA Strategic Support Information Engineering University. His main research interests include antennas and propagation.



**Jun Gao** received his BS degree from PLA Strategic Support Information Engineering University, Zhengzhou, China, in 2015. His main research interests include aperture antennas, high-gain antennas, and beam-steering antennas.



**Mingyang Zhao** obtained his bachelor degree in electromagnetic field and microwave technology from the University of Information Engineering in 2013, and is currently studying for a Ph.D. in Information and Communication Engineering. His current research interests include phased arrays, antenna array synthesis, and optimization algorithms.